https://doi.org/10.5194/egusphere-2024-2246
Preprint. Discussion started: 19 August 2024

Variations in vegetation evapotranspiration affect water yield in high-altitude areas

Yinying Jiao[1,2,3], Guofeng Zhu[1,2,3*], Dongdong Qiu[1,2,3], Siyu Lu[1,2,3], Gaojia Meng[1,2,3], Rui Li[1,2,3],Qinqin Wang[1,2,3], Longhu Chen[1,2,3], Wentong Li[1,2,3]

[1]College of Geography and Environment Science, Northwest Normal University, Lanzhou 730070, Gansu, China
[2]Shiyang River Ecological Environment Observation Station, Northwest Normal University, Lanzhou 730070, Gansu, China
[3]Key Laboratory of Resource Environment and Sustainable Development of Oasis, Gansu Province, Lanzhou 730070, Gansu, China

Correspondence to: Guofeng Zhu (zhugf@nwnu.edu.cn)

Abstract. Global mountains and plateaus are the main water-producing areas on land. However, under the influence of climate change, the distribution of vegetation and the way water is utilized in these areas have undergone significant changes. As such, understanding the effects of evapotranspiration from high-altitude vegetation on precipitation and runoff is vital in addressing the uncertainties and challenges posed by climate change. Between 2018 and 2022, we conducted research in the northeastern Qinghai-Tibet Plateau, collecting data on precipitation, soil water, and Picea crassifolia xylem water to quantify the impact of vegetation transpiration and recirculated water vapor on precipitation. Our findings indicate that transpiration from vegetation accounts for the largest share of evapotranspiration within the entire forest ecosystem, averaging 57%. Therefore, vegetation transpiration is the decisive factor in determining the water yield of inland high-altitude areas. The average contribution of local evapotranspiration to precipitation reaches 28%, making it the main driver behind the increase in precipitation at high altitudes. The warming of global temperatures and human activities are likely to induce shifts in the distribution areas and evapotranspiration regimes of alpine vegetation, potentially altering water resource patterns in the basin. It is necessary to actively adapt to the changes in water resources in the inland river basin.

1 Introduction

Projected future scenarios suggest that drought events will become more frequent, severe, and prolonged due to the effects of climate change. This phenomenon is expected to manifest most rapidly and intensely in arid and semi-arid regions (Ault et al., 2020). Large-scale forest ecosystems play a pivotal role in influencing climate through biophysical feedback mechanisms and in altering the global water cycle. Notably, an increase in evapotranspiration and the content of inland advection water vapor contributes to a rising trend in global land water storage. This increase in evapotranspiration, crucial for the replenishment of precipitation, is vital for the sustenance and growth of mountain vegetation (Jasechko et al., 2013). The Picea crassifolia ecosystem, providing a range of ecological, climatic, and social benefits to the northeastern Tibetan Plateau, exhibits high susceptibility to drought and temperature extremes. Furthermore, climate-related drivers significantly heighten

https://doi.org/10.5194/egusphere-2024-2246
Preprint. Discussion started: 19 August 2024

the vulnerability of Picea crassifolia to drought and heat stress, with an anticipated increase in disturbances to its ecosystem as climate change progresses. The dynamic interaction between soil and vegetation is instrumental in regulating precipitation inputs and water transfers within ecosystem components, thus positioning it as a critical factor in climate change mitigation through its climatic benefits (Rohatyn et al., 2022).

The evaluation of the evapotranspiration ratio within forest ecosystems, particularly in the complex mountainous environments, cannot be conducted in isolation due to the intricate interplay of various factors (Li et al., 2023). Variations in evaporation loss are known to precipitate disturbances in the precipitation and surface water budget, alongside alterations in soil moisture dynamics and the processes governing snowmelt. The upward movement of water vapor in the atmosphere, upon merging with advection water vapor, condenses to form precipitation. This phenomenon is more pronounced in high-altitude areas, which are characterized by greater vegetation coverage and favorable conditions for the confluence of water vapor, resulting in more abundant precipitation. The trajectory and intensity of the westerly winds play a pivotal role in determining the moisture content and, consequently, the distribution of precipitation across the high mountains of Central Asia, predominantly under the influence of the subtropical westerly jet during the cold season (Mehmood et al., 2022). Moreover, even minor adjustments in the allocation of atmospheric water can trigger significant shifts in latent heat, atmospheric circulation, water transport, and precipitation patterns (Hao et al., 2023).

As a vascular plant species, Picea crassifolia plays a crucial role in channeling energy and materials from the environment into terrestrial ecosystems. Its growth, survival, and reproduction significantly influence the ecological functions and structures of other species, both within their habitats and in broader ecological contexts. A significant interaction exists between the vegetation, its drought resilience, and the microclimatic conditions within forests and their ecosystems. This interaction is vital for understanding ecosystem dynamics (Eisenhauer et al., 2021). In this study, we conducted monthly observations and analyses of the xylem water potential, soil water potential, stable isotopes of precipitation, and soil water content of Picea crassifolia in the northeastern Qinghai-Tibet Plateau from April to October for the years 2018 and 2022. These data were utilized to address the following research objectives: (1) To quantify the contribution rates of soil evaporation and vegetation transpiration to the total evapotranspiration of ecosystems; (2) To determine the ratio of recirculated water vapor in precipitation; and (3) To investigate the evapotranspiration process and its impact on productivity and hydrological convergence in the forest belt of the mountainous region. This study provides a robust foundation for the management of local water resources and the protection of ecological integrity.

2 Study area

The Qilian Mountains are located in the central part of the Eurasian continent, on the northeastern edge of the Qinghai-Tibet Plateau(Figure 1). The eastern region is dominated by water erosion, with large variations in mountainous terrain and an average elevation of over 4,000 meters. Permafrost is developed at elevations of 3,500 to 3,700 meters, and areas above 4,500 meters are characterized by modern glacier development. The region has a plateau continental climate, with hot

https://doi.org/10.5194/egusphere-2024-2246
Preprint. Discussion started: 19 August 2024

summers and cold winters, strong solar radiation, and large temperature differences between day and night. The average annual temperature is below 4℃, with extreme highs of 37.6℃ and extreme lows of -35.8℃. The annual sunshine hours range from 2,500 to 3,300 hours, with a total solar radiation of 5,916 to 15,000 megajoules per square meter. The average annual precipitation is 400 millimeters, and the annual evaporation ranges from 1,137 to 2,581 millimeters. The average wind speed is around 2 meters per second, and the frost-free period lasts from 23.6 to 193 days. The Shiyang River originates from the Daxueshan on the northern side of the Lenglong Ridge in the eastern section of the Qilian Mountains, serving as a major water source for the city of Wuwei. The soil types in the eastern section are diverse, but with low organic matter content. The distribution of vegetation shows distinct zonal characteristics, with mountainous forest-grassland zones (2,600 to 3,400 meters), subalpine shrub-meadow zones (3,200 to 3,500 meters), and high mountain sub-ice-snow sparse vegetation zones (>3,500 meters) at elevations above 2,700 meters. The main types of natural forest vegetation include Picea crassifolia, Qilian juniper forest, and Chinese pine forest, with Picea crassifolia being the dominant tree species (Zhu et al., 2022).

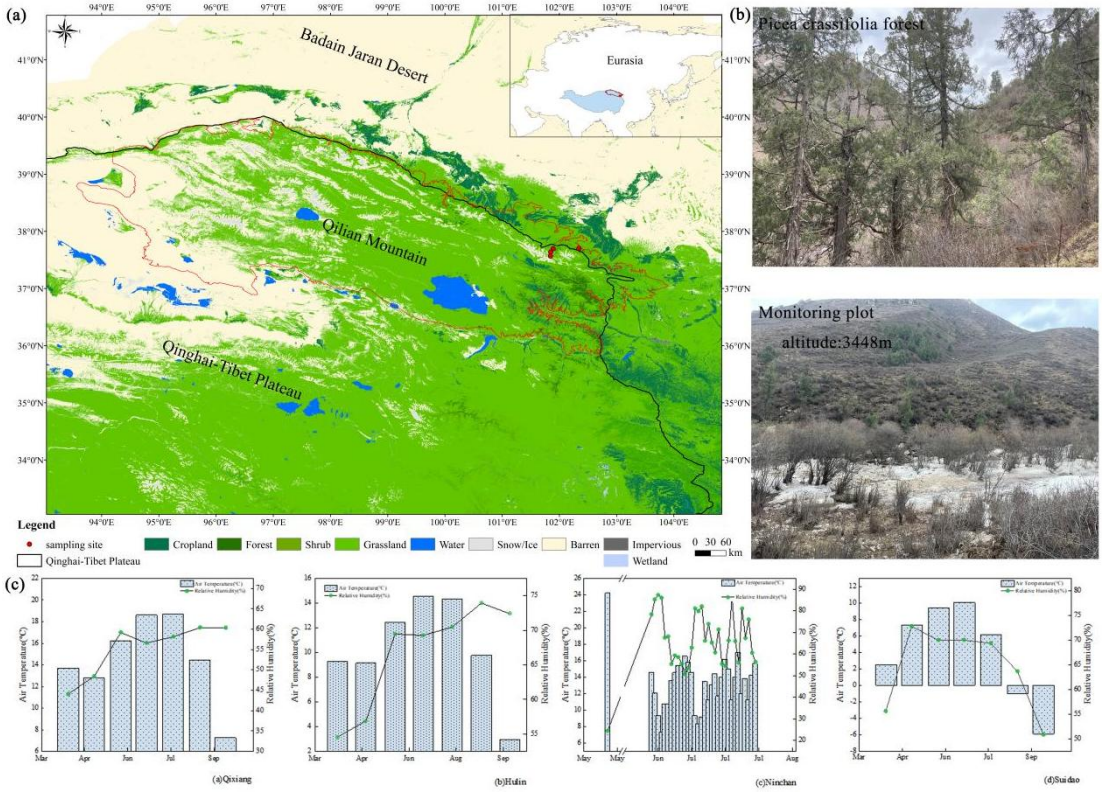

Figure 1:Location of the study area and changes in meteorological conditions.

https://doi.org/10.5194/egusphere-2024-2246
Preprint. Discussion started: 19 August 2024

3 Materials and methods

3.1 Materials Sources

In this study, we established a stable isotope observation network at four elevation zones (2543m, 2721m, 3068m, 3448m) in terms of vertical height (Table 1). Meteorological data were recorded using an automatic weather station in the years 2018 and 2022, incorporating a rain gauge for precipitation collection. The collected precipitation was subsequently transferred to 100ml containers following each rainfall event. Soil samples were extracted from the sample plot at various depths, specifically at intervals of 0-5 cm, 5-10 cm, 10-20 cm, 20-30 cm, 30-40 cm, 40-50 cm, 50-60 cm, 60-70 cm, 70-80 cm, 80-90 cm, and 90-100 cm, utilizing a soil drill. These samples were bifurcated, with one portion being stored in a 50 ml glass bottle. This bottle was hermetically sealed with a parafilm and transported to the observation station, where it was marked with the sampling date and subjected to cryopreservation within 10 hours for the purpose of stable isotope analysis. The remaining portion of the soil sample was placed in a 50ml aluminum box to ascertain soil moisture content through a drying method. For the collection of plant samples, scissors were employed to harvest the xylem stems of vegetation. The bark was removed, and the samples were placed in 50ml glass bottles, which were then sealed and frozen for subsequent experimental analysis.

Table 1:Sampling location and sampling quantity information during the growing season.

Parameter	Station	Qixiang	Hulin	Ninchan	Suidao
	Altitude(m)	2543	2721	3068	3448
Local climate	Temperature(℃)	3	3.2	3.3	-0.9
	Precipitation(mm)	262	370	394	475
	Relative humidity（%）	52.9	56.1	66.6	69.2
Samplings number	Precipitation	53	108	91	135
	Soil water	220	560	560	560
	Xylem water	236	56	56	56

We employed the monthly potential evapotranspiration dataset for China, characterized by a spatial resolution of approximately 1 km (0.0083333°), spanning the period from January 1990 to December 2021. Measurements are expressed in units of 0.1 mm. This dataset is synthesized from the China 1 km monthly mean, minimum, and maximum temperature datasets (Ding et al., 2020; Ding et al., 2021), utilizing the Hargreaves equation to estimate potential evapotranspiration (Peng et al., 2017). The equation employed is as follows: $PET = 0.0023 \times S0 \times (MaxT - MinT)0.5 \times (MeanT + 17.8)$, where PET denotes the potential evapotranspiration in mm/month. Here, MaxT, MinT, and MeanT represent the monthly maximum, minimum, and mean temperatures, respectively. S0 is the theoretical solar radiation incident at the top of the Earth's atmosphere, calculated considering the solar constant, the Earth-sun distance, the Julian day, and the latitude. For the sake of storage efficiency, data are encoded as int16 within NETCDF (nc) files. Additionally, surface evapotranspiration

https://doi.org/10.5194/egusphere-2024-2246
Preprint. Discussion started: 19 August 2024

data were sourced from the MODIS-based daily surface evapotranspiration dataset for the Qilian Mountains (2019), which features a spatial resolution of 0.01° (Yao et al., 2017).

3.2 Experimental Analysis

The isotopic data used in this study mainly include stable isotopes of precipitation, soil water, and xylem water. All isotopic samples were analyzed at the Stable Isotope Laboratory of Northwest Normal University. The precipitation samples were analyzed for hydrogen and oxygen stable isotopes using a liquid water isotope analyzer (DLT-100, Los Gatos Research, USA). After thawing the soil and vegetation samples, they were extracted using a low-temperature vacuum condensation device (LI-2100, LICA United Technology Limited, China), and the extracted water was subjected to isotopic analysis. Each water sample was tested six times to ensure accuracy, with the first two tests considered as interference and only the results of the subsequent four tests were averaged (Zhu et al., 2022). The isotopic measurements are represented by δ, which represents the deviation in parts per thousand of the ratio of two stable isotopes in the sample relative to the ratio in a standard sample. The International Atomic Energy Agency (IAEA) defined the Vienna Standard Mean Ocean Water (VSMOW) in 1968 as the standard for isotopic composition, which is derived from distilled seawater and has a similar isotopic composition to Standard Mean Ocean Water (SMOW).

$$\delta = \left(\frac{\delta_{Sampling}}{\delta_{Standard}} - 1\right) \times 1000‰ , \quad (1)$$

3.3 Research methods

3.3.1 Isotopic composition of atmospheric water vapour

The stable isotope composition of moisture in ambient air is calculated as follows(Gibson and Reid, 2014;Skrzypek et al., 2015):

$$\delta_A = \frac{\delta_{rain} - k\varepsilon^+}{1 + k\alpha^+ \times 10^{-3}} , \quad (2)$$

where k=1, or by fitting k to some fraction of 1 as the best fit to the local evaporation line, is the isotopic fractionation factor. Defined by. about ^{2}H and ^{18}O are calculated as follows(Horita and Wesolowski, 1994):

$$10^3 \ln^2\alpha^+ = 1158.8T^3/10^9 - 1620.1T^2/10^6 + 794.84T/10^3 - 161.04 + 2.9992 \times 10^9/T^3 , \quad (3)$$

$$10^3 \ln^{18}\alpha^+ = -7.685 + 6.7123 \times 10^3/T - 1.6664 \times 10^6/T^2 + 0.35041 \times 10^9/T^3 , \quad (4)$$

Here, α^+ is the equilibrium fractionation factor dependent on temperature, and T is the temperature (K).

https://doi.org/10.5194/egusphere-2024-2246
Preprint. Discussion started: 19 August 2024

3.3.2 Isotopic composition of soil evaporation

The Craig-Gordon model was used to calculate the stable isotopic composition of soil evaporation water vapour, δE, using the following equation(Yepez et al., 2005).

$$\delta_E = \frac{\alpha_e^{-1}\delta_s - h\ \delta_A - \varepsilon_{eq} - (1-h\ )\varepsilon_k}{(1-h\ ) + 10^{-3}(1-h\ )\varepsilon_k}, \quad (5)$$

where αe(>1) is the equilibrium factor calculated as a function of water surface temperature, δs is the stable isotopic composition of liquid water at the evaporating surface of the soil (0 ~ 10 cm average stable isotopic composition of soil water), δA is the stable isotopic composition of atmospheric water vapour near the surface, Ɛeq represents the equilibrium fractionation corresponding to Ɛeq = (1-1/αe) × 1000, ε_k is the kinetic fractionation factor of oxygen is approximately 18.9‰ and h is the atmospheric relative humidity(Gibson and Reid, 2010). For δ18O, αe is calculated as follows(Raz-Yaseef et al., 2010):

$$\alpha_e = \frac{1.137\times10^6/T^2 - 0.4156\times10^3/T - 2.0667}{1000} + 1, \quad (6)$$

Where T is the soil Kelvin temperature (K) at a depth of 5 cm.

3.3.3 Isotopic composition of plant transpiration

When transpiration is strong, leaf water is in "isotopic stable state", that is, the isotopic composition of leaf transpiration water is equivalent to that of water absorbed by the roots of rain plants at noon. Therefore, the stable isotopic composition of water in plant xylem can be used to represent the stable isotopic composition of water vapor in plant transpiration. The expression is as follows(Aron et al., 2020):

$$\delta_T = \delta_X, \quad (7)$$

where δx is the isotopic ratio of xylem water and δT is the isotopic ratio of transpiration.

3.3.4 Evapotranspiration isotope assessment

The Keeling Plot model describes the linear relationship between the oxygen isotope composition of atmospheric water vapour and its reciprocal concentration . The intercept of the curve on the Y-axis represents the oxygen isotopic composition of evapotranspiration (δ_{ET}) and is expressed as(Keeling, 1958;Wang et al., 2015)：

$$\delta_a = \frac{C_b(\delta_b - \delta_{ET})}{C_a} + \delta_{ET}, \quad (8)$$

Where δa and Ca represent the atmospheric water vapour oxygen isotopic composition (‰) and water vapour concentration in the ecosystem boundary layer, δb and Cb represent the background atmospheric water vapour oxygen isotopic

https://doi.org/10.5194/egusphere-2024-2246
Preprint. Discussion started: 19 August 2024

composition and background atmospheric water vapour concentration, and δ_{ET} is the ecosystem evapotranspiration oxygen isotopic composition.

3.3.5 Proportion of vegetation transpiration

The determination of evapotranspiration by means of biotic and abiotic isotopic composition can be used to improve the understanding of community structure and ecosystem function in picea crassifolia in the northeastern of Tibetan Plateau. Based on the isotope mass balance approach to consider the distribution of major and minor isotopes, the partitioning of evapotranspiration can be achieved using two end-member mixing models (E and T) with the following expression(Kool et al.,2014;Wei et al., 2018):

$$\frac{T}{ET} = \frac{\delta_{ET}-\delta_E}{\delta_T-\delta_E}, \quad (9)$$

where δ_{ET}, δ_E and δ_T are the isotopic compositions of evapotranspiration (ET), soil evapotranspiration (E) and plant evapotranspiration (T), respectively, and the isotopic values of the three can be obtained by both direct observation and model estimation.

3.3.6 Bayesian mixing model

Assuming that precipitation vapor is a mixture of advective water vapour and recirculating water vapour, it is understood that the proportion of both precipitation and precipitation water vapour has the same nature. The proportion of precipitation occupied by advective vapour is calculated as follow(Kong et al., 2013; Wang et al., 2022):

$$f_{re} = \frac{P_{tr}+P_{ev}}{P_{tr}+P_{ev}+P_{adv}}, \quad (10)$$

where Ptr, Pev and Padv are precipitation produced by transpiration, surface evaporation and advection, respectively.

This can be calculated using the following formula(Brubaker et al., 1993; Sang et al., 2023):

$$\delta_{pv} = \delta_{tr}f_{tr} + \delta_{ev}f_{ev} + \delta_{adv}f_{adv}, \quad (11)$$

$$f_{ev} + f_{tv} + f_{adv} = 1, \quad (12)$$

where *f*tr, *f*ev and *f*adv are the proportional contributions of transpiration, surface evaporation and advection to precipitation, respectively, and δpv, δtr, δev and δadv values are the stable isotopes in precipitating transpiration, transpiration, surface evaporation and advective vapour, respectively. δpv is calculated using the following formula:

$$\delta_{pv} = \frac{\delta_p - k\varepsilon^+}{1+k\varepsilon^+}, \quad (13)$$

Using the C-G model to calculate δev, the formula is as follows:

$$\delta_e = \frac{\delta_s/\alpha^+ - h\delta_{adv} - \varepsilon}{1-h+\varepsilon_k}, \quad (14)$$

Including the δs is the isotopic composition of liquid water evaporation front, δadv is advection steam, h is relative humidity, α^+ is equilibrium fractionation factor, ε_k is kinetic fractionation factor, ε is total fractionation factor.

https://doi.org/10.5194/egusphere-2024-2246
Preprint. Discussion started: 19 August 2024

$$\varepsilon = \varepsilon^{+}/\alpha^{+} + \varepsilon_{k}\,, \tag{15}$$

$$\varepsilon_{k} = (1-h)\theta_{n}C_{k}\,, \tag{16}$$

h is the relative humidity, C_k is the kinetic fractionation constant, δ^2H is 25.1‰, $\delta^{18}O$ is 28.5‰.The weight coefficient θ of small water body is 1, and θ of large water body is 0.5. n ranges from 0.5 (fully turbulent transport, with reduced kinetic fractionation, suitable for lake or saturated soil conditions) to 1 (fully diffused transport, suitable for very dry soil conditions), with a kinetic fractionation coefficient of about 12.2-24.5‰ for ε_k (^2H) in a dry atmosphere (h=0). The kinetic separation coefficient of ε_k (^{18}O) is about 13.8-27.7‰.

The advection water vapor isotope δadv in the three-component mixing model needs to be determined by the water vapor isotopic composition at the upwind position. Based on the HYSPLIT model, we found that the northeastern of Tibetan Plateau was controlled by westerly winds, southeast monsoon and plateau monsoon in June, July and August, and by prevailing westerly winds in September and October. The clustering analysis of air masses in different months shows that air masses accumulate at the northern foot of Qilian Mountains and move from low altitude to high altitude along the valley. Xiying, at 2097 m above sea level, is therefore used as a headwind station from April to October. When steam isotopes show a depletion trend along the transport path, isotopic fractionation is assumed to be due to Rayleigh distillation, and the expression is as follow:

$$\delta_{adv} = \delta_{pv-adv} + (\alpha^{+}-1)\ln F\,, \tag{17}$$

Where δpv-adv is the isotopic composition in the vapor of the winds tation, and F is the ratio between the final vapor and the initial vapor. Since rainfall is positively correlated with the surface vapor pressure of the whole study area (c=1.657e, where c is the water vapor content in mm, e is the surface vapor pressure in hPa, R^2=0.94), we used the surface vapor pressure of each site to calculate the value of F.

4 Results and analysis

4.1 Hydrogen and oxygen isotope variations in different water bodies

During the growth season of Picea crassifolia, precipitation stable isotopes display distinct fluctuation patterns(Table 2). In the initial growth phase, the hydrogen and oxygen isotope ratios exhibit relatively low values. With the progressive rise in temperature, the rate of water evaporation and subsequent loss escalates, resulting in an isotopic enrichment. The mean δ^2H value in precipitation throughout the growth season is recorded at -45.52‰, with fluctuations ranging from -151.88‰ to 63.43‰. Similarly, the mean $\delta^{18}O$ value stands at -7.75‰, exhibiting fluctuations between -31.49‰ and 14.79‰. The isotopic composition in the wood tissues does not show significant depletion or enrichment, displaying a fluctuation range from -76.95‰ to 23.87‰ for δ^2H and from -11.92‰ to 24.77‰ for $\delta^{18}O$. Compared to precipitation and wood tissues, shallow soil water demonstrates a lesser enrichment of heavy isotopes, with a reduced fluctuation extent observed during the late spring and early summer period.

https://doi.org/10.5194/egusphere-2024-2246
Preprint. Discussion started: 19 August 2024

Table 2:Stable isotopes of different water bodies during the growing season.

Average / Period	δ^2H/‰			$\delta^{18}O$/‰		
	Precipitation	Xylem water	Soil water (0~10cm)	Precipitation	Xylem water	Soil water (0~10cm)
April	-69.15	-39.02	-53.10	-10.25	2.56	-7.10
May	-39.09	-29.78	-45.38	-7.61	4.44	-6.42
June	-31.29	-45.83	-46.08	-5.74	-2.83	-6.12
July	-32.39	-47.63	-47.71	-5.33	-0.97	-7.06
August	-48.88	-44.55	-68.85	-7.79	-2.06	-9.07
September	-29.38	-42.62	-49.20	-6.46	-1.83	-6.79
October	-68.43	-44.57	-54.88	-11.06	-2.25	-7.96

Variations in the Local Meteoric Water Line (LMWL) across different vertical gradients are primarily influenced by temperature and humidity. Notably, relative humidity remains consistently low at all four measured elevations within the forest, causing the LMWL to be lower than the Global Meteoric Water Line (GMWL). At an elevation of 2543 meters, which marks the lowest tree growth layer, temperatures can reach up to 20℃ in July, with the LMWL showing a slope of 6.74. At 2721 meters, the average temperature during the growing season is 10.4℃, peaking at 16.45℃ in July and an average relative humidity of 64.38%. The slope of the LMWL at this elevation is 7.02(Figure 2d). At the Suidao station, located at an elevation of 3448 meters, the slope of the precipitation regression line is 7.75. This value is close to the GMWL's slope but exhibits the largest deviation from the local evaporation line, as depicted in (Figure 2a). In the forest's lower layer, the Soil Water Line (SWL) is narrower and closer to the local evaporation line, indicating more pronounced evaporative fractionation and dynamic fractionation compared to the other three sampling zones. The SWL slopes are less steep than those of the LMWL, indicating that precipitation is the primary source of soil moisture replenishment.

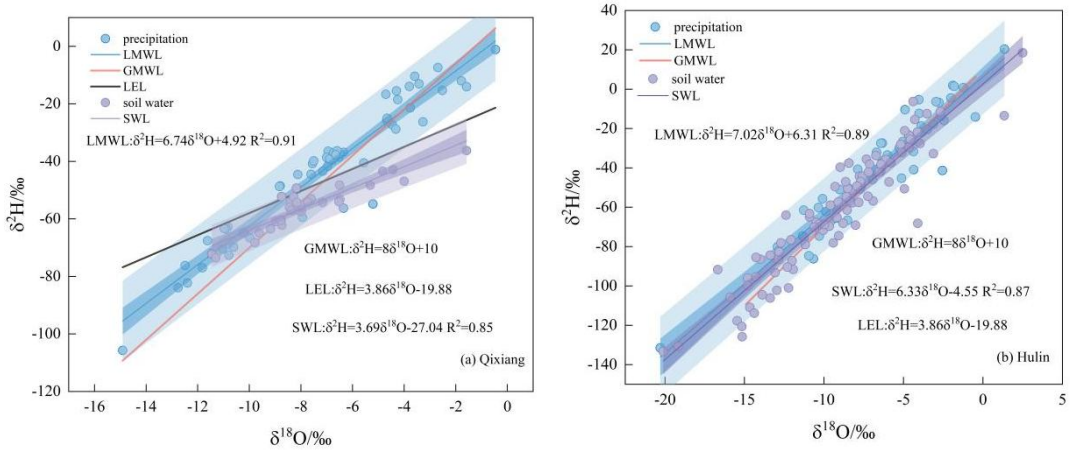

https://doi.org/10.5194/egusphere-2024-2246
Preprint. Discussion started: 19 August 2024

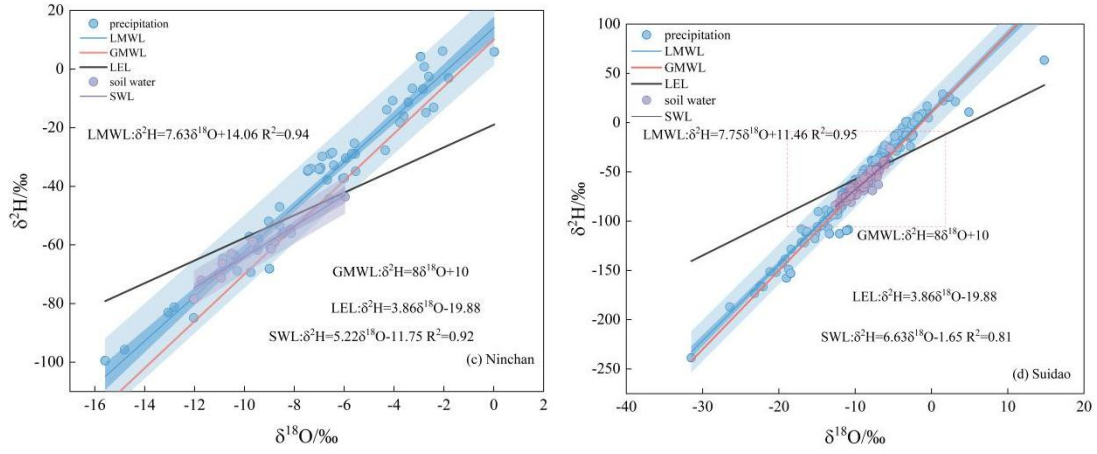

Figure 2:(a) Qixiang, (b) Hulin, (c) Ninchan, (d) Suidao. Compare the distributions and fittings of precipitation and soil water stable isotopes at the four locations.

During the precipitation process, unsaturated water vapor leads to non-equilibrium fractionation, as indicated by an average d-excess value of 16.58‰ throughout the growing season (Figure 3a). In May and September, the evaporation rate of water vapor increases due to relatively higher humidity levels compared to other periods. From June to August, the fluctuations in deuterium values are gradual; however, significant variations begin from mid-August onwards. This trend suggests that local evaporation intensifies over time, influenced by temperature and relative humidity, resulting in increased rates of non-equilibrium evaporation. The average lc-excess value of precipitation at the lower elevation of forest distribution is recorded at -8.18‰. In contrast, the average lc-excess values in the precipitation at the middle, upper-middle, and canopy layers of the forest are approximately 0. This difference indicates that the evaporation fractionation effect is more pronounced at lower elevations due to direct exposure to environmental conditions. At higher elevations, the soil moisture content across all soil layers remains above 30%, influenced by rainfall and snowmelt (Figure 3b). By the end of the growing season, decreasing temperatures lead to leaf fall, resulting in the formation of a litter layer on the forest floor. This layer plays a pivotal role in retaining soil moisture, underscoring the dynamic interactions between vegetation, soil, and atmospheric conditions throughout the season.

https://doi.org/10.5194/egusphere-2024-2246
Preprint. Discussion started: 19 August 2024

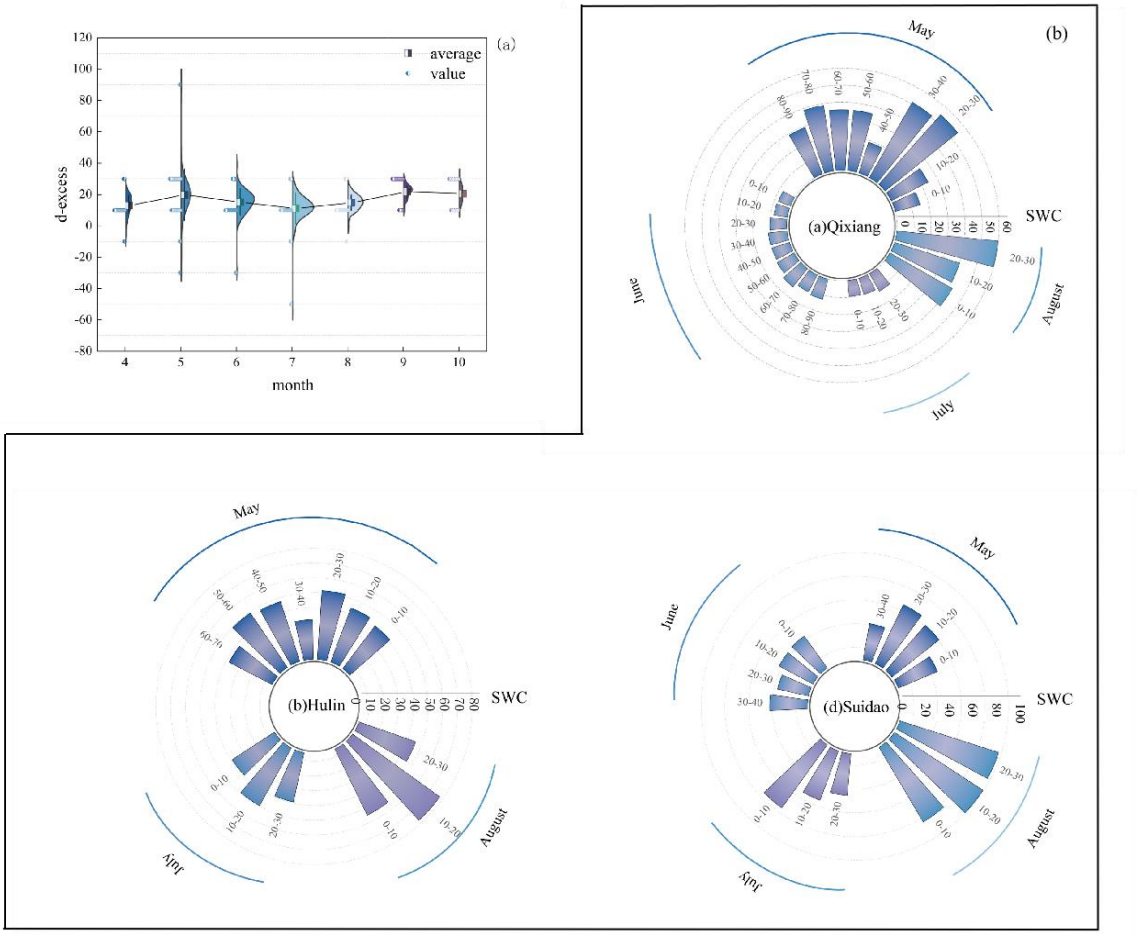

Figure 3:(a) Variation in soil water content, (b) Comparison between atmospheric water vapour oxygen isotopes and d-excess.

4.2 Soil evaporation, plant transpiration and ecosystem evapotranspiration

Table 3:Evaporation and transpiration at different altitudes during the growing season（* represents missing value）.

Site	Type	April	May	June	July	August	September	October
Qixiang	δ_T	2.22	-5.87	-4.59	-0.72	-1.72	-1.78	-2.26
	δ_E	-30.32	-28.68	-27.33	-29.12	-28.68	-26.32	-27.27
	δ_{ET}	-20.19	-20.05	-11.63	-9.87	-13.56	-15.85	-21.56
Hulin	δ_T	-5.34	-3.58	-4.13	-0.34	-2.35	-4.25	-1.97
	δ_E	-29.68	-27.28	-25.8	-27.75	-24.56	-25.21	-27.88
	δ_{ET}	-21.59	-22.36	-8.93	-10.17	-11.57	-18.8	*
Ninchan	δ_T	*	-3.45	-1.98	-1.05	-6.68	*	*
	δ_E	*	-20.57	-26.31	-29.08	-18.22	-18.15	-18.22
	δ_{ET}	*	*	-12.46	-7.57	*	*	*

https://doi.org/10.5194/egusphere-2024-2246
Preprint. Discussion started: 19 August 2024

	δ_T	*	-8.45	-6.98	-6.05	-6.68	*	*
Suidao	δ_E	-29.79	-27.32	-27.91	-23.83	-28.78	-25.8	-28.06
	δ_{ET}	-24.31	-16.14	-15.19	-10.07	-18.05	-23.02	-18.65

The Keeling plot method was used to analyze the stable isotope composition of ecosystem evapotranspiration (Figure 4). Its principle involves linearly fitting the water vapor concentration in the ecosystem boundary layer against the oxygen isotope composition, with the intercept on the y-axis representing the stable isotope value of δ_{ET}. The results indicate that at different heights within the distribution of deciduous trees, the average δ_{ET} value is -22.59‰. Throughout the entire growing season, δ_{ET} does not consistently decrease with increasing elevation. Specifically, near the treeline, there are higher stable isotope values, but in the middle and upper layers of the forest, there is a minimal value, indicating lower and less stable isotopic fractionation in that layer. At an elevation of 3448m, as the number of deciduous trees decreases and shrubs become dominant, the δ_{ET} value is -21.81‰(Table 3). We found that the stable isotope δ_E of soil evaporation at depths of 0-10cm is more enriched at lower elevations, particularly in April and May when the isotopic enrichment is more pronounced. From June to August, due to a significant increase in vegetation coverage, soil evaporation intensity decreases. In the early stage of the growing season, when leaves have not fully developed, the stable isotope composition of the xylem exhibits a relatively depleted characteristic. In July and August, when leaves are fully expanded, temperatures rise, and the rainy season in mountainous areas commences, transpiration becomes more intense.

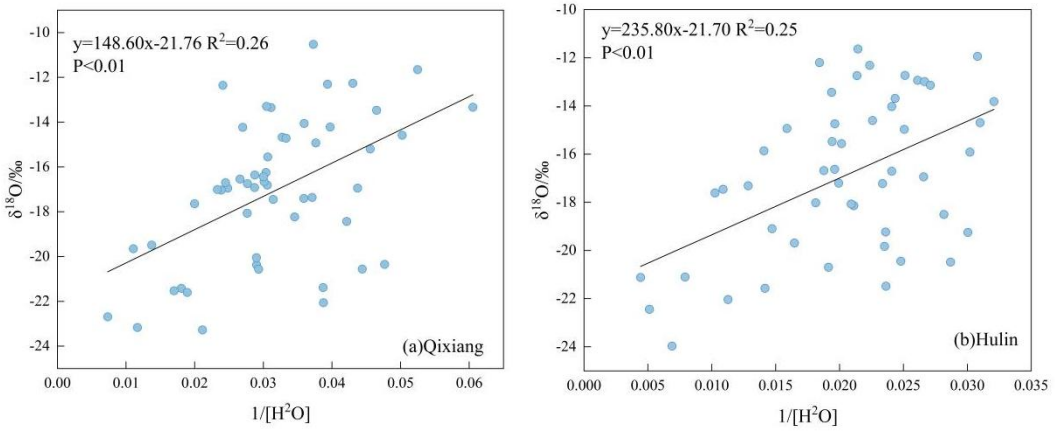

https://doi.org/10.5194/egusphere-2024-2246
Preprint. Discussion started: 19 August 2024

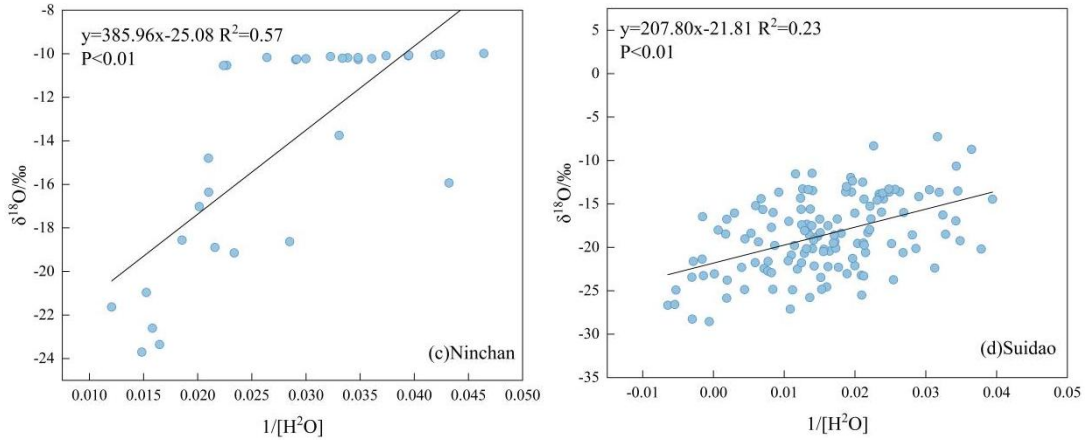

Figure 4:Each sampling point is fitted with a trend line based on the Keeling plot method.

4.3 T/ET assessment of picea crassifolia ecosystem in different months

We found that the canopy closure of deciduous trees significantly influences the evapotranspiration of the entire ecosystem (Figure 5). In April and May, as temperatures rise, surface vegetation exhibits weaker growth, resulting in a higher proportion of soil evaporation within the ecosystem, while transpiration by vegetation remains relatively low. During the rainy season in June to August, vegetation experiences vigorous growth, and transpiration reaches its peak in July. In September and October, soil evaporation becomes more dominant as temperatures, relative humidity, and rainfall gradually decrease, and deciduous tree leaves become wilted. At lower elevations, the T/ET ratio fluctuates between 0.20 and 0.70 in a distinct pattern, while above the treeline, transpiration ratios fluctuate between 0.20 and 0.80 in a similar pattern. Overall, summer is characterized as the peak season for transpiration, with a minimal contribution from soil evaporation.

https://doi.org/10.5194/egusphere-2024-2246
Preprint. Discussion started: 19 August 2024

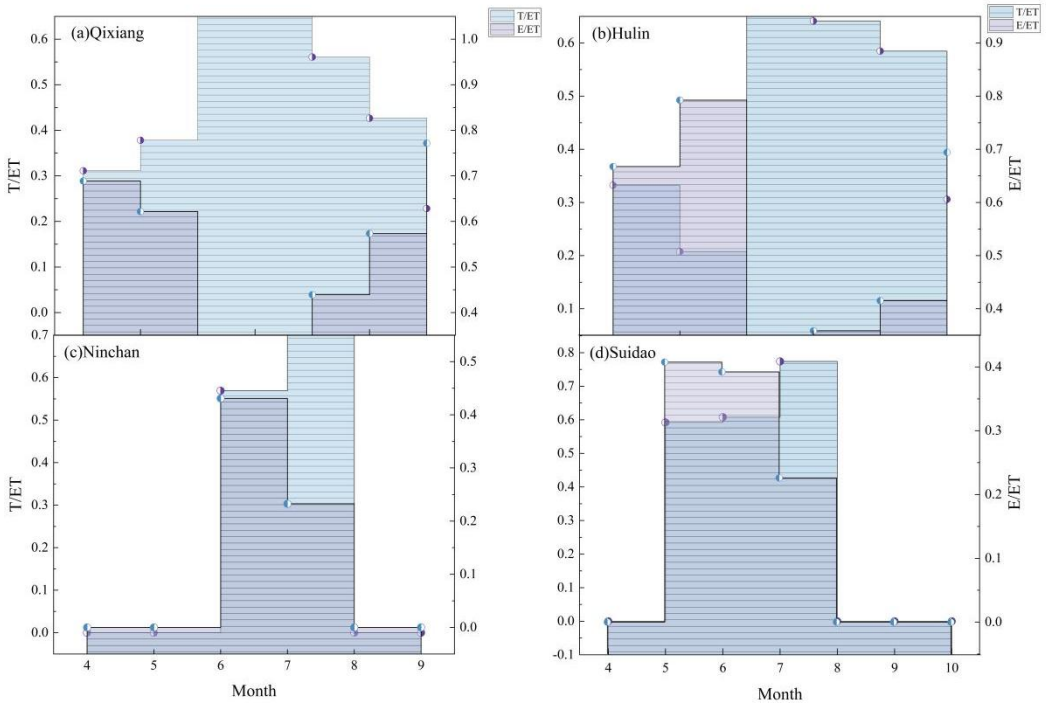

Figure 5:The proportion of soil evaporation and vegetation transpiration in evapotranspiration of ecosystem(0 represents missing value).

5 Discussions

5.1 Hydrological effects of changes in evapotranspiration

5.1.1 Contribution to recirculating water vapour in precipitation

Our previous study in the northeastern of Tibetan Plateau (Zhang et al., 2021) indicated that above an altitude of 2100m, air masses gather from the northern foothills and move along the valley from low to high elevations. From June to August, the atmospheric circulation is influenced by westerlies, southeast monsoons, and plateau monsoons, while from September to October, the westerlies are the dominant factor. Therefore, we selected the Xiying station at an altitude of 2097m as our upwind site. The δpv values showed depletion in April and October, gradually enriching from June to August. The maximum δ^2H value was -76.02‰ (Table 5), and the minimum was -184.93‰, while the maximum $\delta^{18}O$ value was -11.89‰, and the minimum was -26.38‰. Above 2700 meters, there is a gradual decrease in precipitation vapor with increasing altitude. The δev values exhibited significant fluctuations throughout each month, with different patterns at different locations. At 2721m, the δev range varied between -172.3‰ and 96.39‰. From the forest's lower layer to the upper layer, the isotopic composition of the advected moisture from the valley gradually diminished, resulting in decreasing values of δadv.

https://doi.org/10.5194/egusphere-2024-2246
Preprint. Discussion started: 19 August 2024

Table 5:Isotopic Composition of Precipitation Vapor, Surface Evaporation Vapor, and Vegetation Transpiration Vapor at Different Months and Altitudes(- represents missing value).

Month	Type	isotope	April	May	June	July	August	September	October
Qixiang	δpv	δ^2H/‰	-141.95	-123.83	-99.87	-115.99	-128.34	-120.9	-152.43
		$\delta^{18}O$/‰	-19.27	-16.58	-14.04	-15.91	-18.6	-17.22	-22.34
	δev	δ^2H/‰	-	-125.69	-123.69	-117.98	-134.57	-	-
		$\delta^{18}O$/‰	-	-30.21	-29.56	-28.62	-31.19	-	-
	δtr	δ^2H/‰	-39.9	-29.32	-46.19	-49.58	-45.15	-42.66	-44.64
		$\delta^{18}O$/‰	2.22	-5.87	-4.59	-0.72	-1.72	-1.78	-2.26
	δadv	δ^2H/‰	-145.57	-83.25	-81.12	-92	-109.62	-100.53	-122.62
		$\delta^{18}O$/‰	-20.24	-11.93	-10.73	-12.06	-15.31	-13.46	-18.16
Hulin	δpv	δ^2H/‰	-129.93	-123.29	-98.68	-113.98	-124.16	-118.52	-164.82
		$\delta^{18}O$/‰	-17.54	-16.62	-13.18	-15.48	-17.33	-17.88	-22.46
	δev	δ^2H/‰	-114.24	-117.01	-107.75	-123.44	-106.92	-96.39	-172.3
		$\delta^{18}O$/‰	-14.77	-16.35	-15.03	-16.7	-14.53	-12.78	-24.82
	δtr	δ^2H/‰	-24.12	-39.62	-35.97	-26.44	-35.85	-38.39	-40.53
		$\delta^{18}O$/‰	-5.34	-3.58	-4.13	-0.34	-2.35	-4.25	-1.97
	δadv	δ^2H/‰	-112.79	-115.67	-106.61	-122.19	-106.49	-95.7	-170.54
		$\delta^{18}O$/‰	-14.59	-16.15	-14.88	-16.54	-14.46	-12.69	-24.57
Ninchan	δpv	δ^2H/‰	-	-76.02	-139.21	-135.74	-129.96	-113.71	-184.93
		$\delta^{18}O$/‰	-	-11.89	-19.87	-18.7	-17.91	-16.77	-26.38
	δev	δ^2H/‰	-	-83.76	-81.42	-92.42	-110.24	-101.11	-123.42
		$\delta^{18}O$/‰	-	-12.01	-10.76	-12.09	-15.37	-13.49	-18.27
	δtr	δ^2H/‰	-	-25.58	-46.77	-37.77	-43.66	-	-
		$\delta^{18}O$/‰	-	-3.45	-1.98	-1.05	-6.68	-	-
	δadv	δ^2H/‰	-162.36	-113.49	-111.45	-106.16	-122.12	-114.67	-141.33
		$\delta^{18}O$/‰	-22.73	-15.94	-15.28	-14.46	-16.96	-16.58	-20.42
Suidao	δpv	δ^2H/‰	-167.86	-128.08	-124.95	-117.32	-137.73	-130.44	-155.52
		$\delta^{18}O$/‰	-22.9	-18.02	-17.28	-16.04	-19.09	-18.64	-21.59
	δev	δ^2H/‰	-164.16	-114.52	-112.37	-106.9	-122.96	-115.47	-142.85
		$\delta^{18}O$/‰	-22.98	-16.07	-15.41	-14.56	-17.08	-16.69	-20.64
	δtr	δ^2H/‰	-	-25.58	-46.77	-37.77	-43.66	-	-
		$\delta^{18}O$/‰	-	-8.45	-6.98	-6.05	-6.68	-	-

https://doi.org/10.5194/egusphere-2024-2246
Preprint. Discussion started: 19 August 2024

δadv	δ^2H/‰	-162.38	-113.51	-111.47	-106.18	-122.14	-114.69	-141.36
	$\delta^{18}O$/‰	-22.73	-15.94	-15.28	-14.47	-16.97	-16.58	-20.42

In July, the ratio of vegetation transpiration to precipitation vapor is significantly higher compared to other months. The temperatures in the lower layers of the forest are relatively high, and the middle to upper layers are densely populated with Picea crassifolia, resulting in a higher *f*tr (transpiration ratio) throughout the entire growing season. Both the early and late stages of the growing season exhibit noticeably higher *f*ev (evaporation ratio) compared to other months, with the middle and upper parts of the forest having a higher proportion of evaporated vapor. The average *f*adv (advected vapor ratio) is 72%, with contributions exceeding 70% for all months except June and July. In mountainous areas, recycled water vapor contributes an average of 28% to precipitation, indicating that the increase in evapotranspiration promotes the occurrence of local precipitation events(Figure 7).

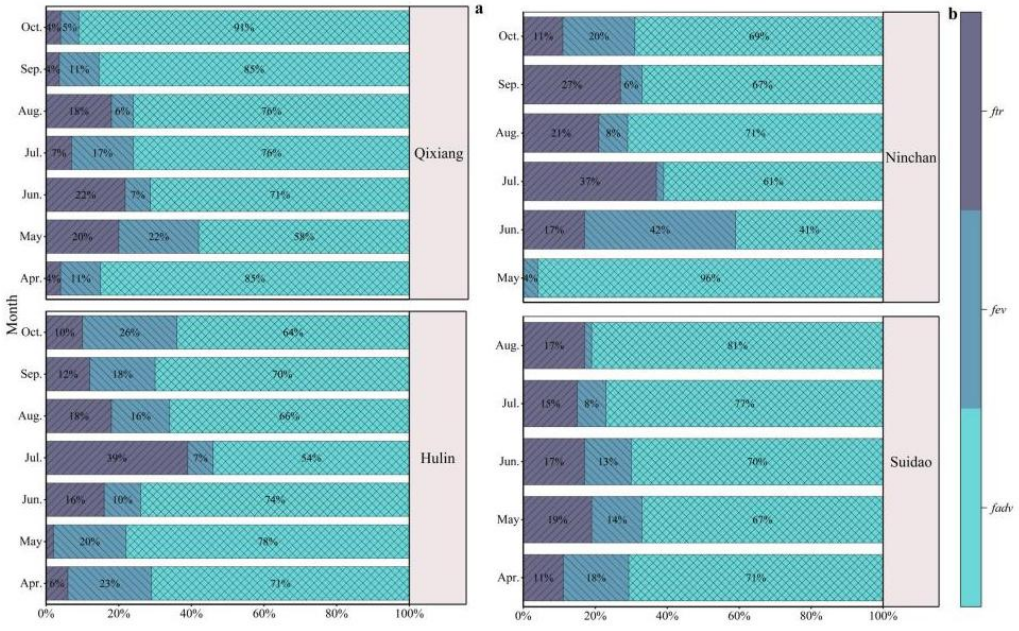

Figure 7:Comparison of fadv (advective water vapour contribution), fev (surface evaporation water vapour contribution) and ftr (plant transpiration water vapour contribution) for each of period.

5.1.2 Impact on surface runoff

Comparing the differences of monthly potential evapotranspiration, surface evapotranspiration and precipitation in picea crassifolia (Table 4), the results clearly showed that rainfall fluctuated between 0-16mm, and the maximum rainfall was 15.7 mm in April, while the minimum value of surface evapotranspiration is 41.8 mm and the minimum value of potential evapotranspiration is 44.1mm. The difference between ETP and ET shows that there is no effective water accumulation in all months. From this, an important conclusion can be drawn: due to the late arrival of the rainy season in mountainous areas and the uneven distribution of rainfall across different altitudinal gradients, surface runoff can not be collected in this area,

https://doi.org/10.5194/egusphere-2024-2246
Preprint. Discussion started: 19 August 2024

which also proves that afforestation in this area will further enhance evapotranspiration, posing a threat to water distribution and utilisation.

Table 4:Month-by-month comparison of potential evapotranspiration, surface evapotranspiration and rainfall.

Variable \ Month	April	May	June	July	August	September	October
ET_p/mm	76.6	87.6	106.5	128.3	118.1	80.0	44.1
ET/mm	51.5	66.3	93.3	108.9	110.7	81.2	41.8
P/mm	15.7	8.8	0	13.2	13.3	11.2	13.6

Some studies suggested that reducing forest density will result in less ET in seasonally dry forests. That reduced ET can be converted into increased groundwater and runoff to supply downstream social water (Wyatt, O'Donnell, & Springer, 2015). It has also been claimed that in some cases, the transient increase in water availability through reduced forest density can actually contribute to subsequent increases in vegetation cover and ultimately reduce runoff (Tague et al., 2019). By assessing the hydrological effects of afforestation through the water cycle in the Asia-Pacific region, it was found that in 7 of the 15 water-deficient areas, positive effects such as increased yield, precipitation, soil moisture and reduced drought risk were achieved through afforestation, and it was confirmed that the water-water cycle had a strong impact and evapotranspiration was increased (Teo et al., 2021). The water vapour content produced by forest transpiration is much higher than that lost by soil surface evaporation, most of the precipitation is intercepted and infiltrated by surface vegetation, and part of the soil water involved in infiltration is absorbed by the root zone of vegetation. Because of plants' high interception and evaporation ability and the absorption of groundwater by root zone, the proportion of transpiration was significantly higher than that of evaporation(Su et al., 2014). In this study zone, upwardly transported advective water vapor progressively diminishes with increasing altitude. The vegetation at elevations from 2500 to 3200 meters supplies abundant evapotranspiration water vapor into the water cycle, the acceleration of which boosts local precipitation(Figure 6). In this case, the groundwater amount decreases gradually with the T value increase. Under the influence of precipitation loss mainly due to plant transpiration, groundwater yield in this region decreases greatly, and has no significant contribution to the downstream water revenue.

https://doi.org/10.5194/egusphere-2024-2246
Preprint. Discussion started: 19 August 2024

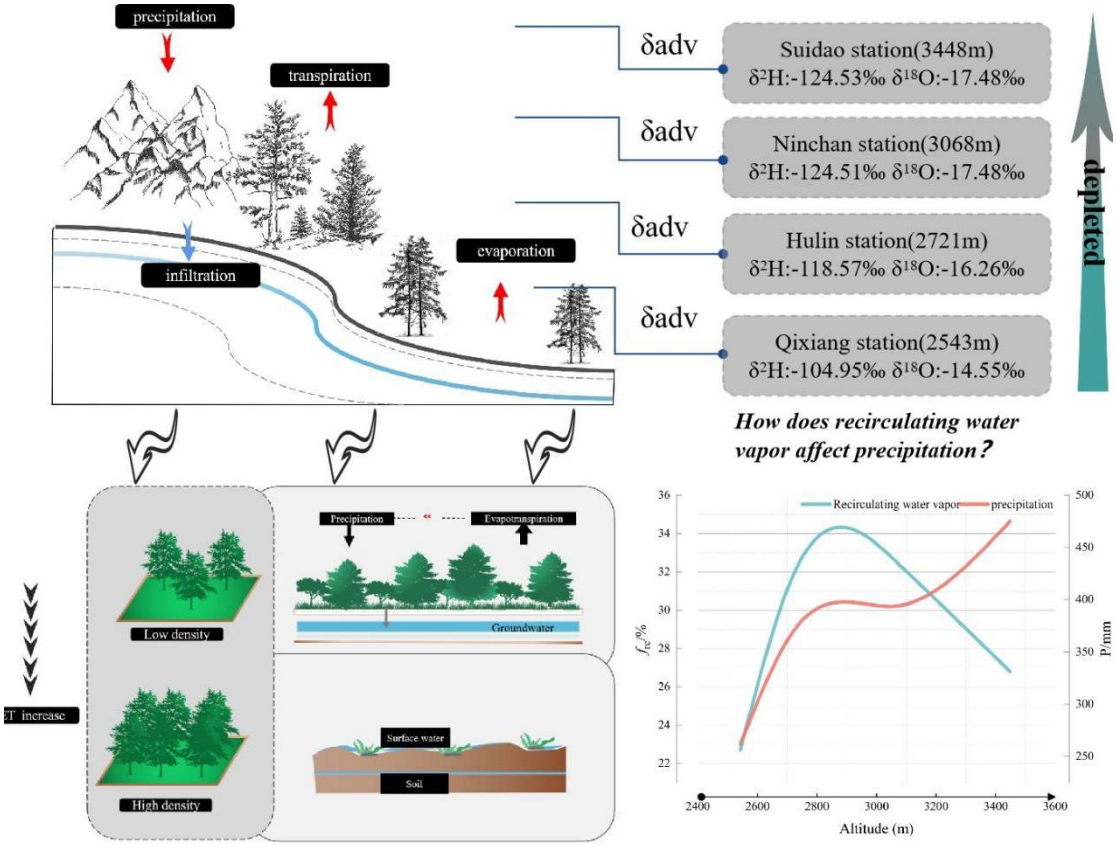

Figure 6:Conceptual model of the hydrological effects of changes in evapotranspiration.

330

5.2 Uncertainty analysis

A higher sample size can reduce the margin of error. Therefore, we utilized isotopic data from four sites over a two-year period to evaluate the model. We used 404 xylem samples to calculate the contribution ratio of transpiration to ecosystem evapotranspiration. We examined the uncertainty of the model evaluation. When analyzing the evaporation characteristics in
335 a semi-arid natural environment using the Craig-Gordon isotopic model, we first eliminated the influence of solar radiation and other meteorological variables on the calculation results. We focused on temperature, relative humidity, water vapor, and the initial isotopic values of water bodies. Particularly in semi-arid environments, the variations in temperature and relative humidity are crucial (Hernández-Pérez et al., 2020). To verify the calculation results, we found a strong correlation between the isotopes of soil evaporation and relative humidity, as demonstrated by the fitting of δE against relative humidity and
340 temperature(Figure 8). This also indicates the reliability of the results obtained through the Craig-Gordon isotopic model. We employed the Keeling plot method to calculate δET, which is based on isotopic mass balance and a two-endmember mixing model. This method assumes that the isotopic composition of the background atmosphere and source remains

https://doi.org/10.5194/egusphere-2024-2246
Preprint. Discussion started: 19 August 2024

constant, with a very low probability of isotopic spatial variation (Good et al., 2012; Kool et al., 2014). Due to the higher reliability of oxygen isotopes compared to hydrogen isotopes (Han et al., 2022; Kale et al., 2022), we solely used oxygen isotopes to calculate the T/ET values. The results indicate that transpiration significantly outweighs evaporation during July and August, which aligns with previous research findings (Zhu et al., 2022). The correlation between T/ET and soil moisture content suggests that soil moisture is a crucial factor driving the variations in transpiration and evaporation ratios. Additionally, the estimation of isotopic composition of advected water vapor from the upwind sites contributes to increased uncertainty. In our study area, the sites are predominantly influenced by valley winds, with water vapor moving from the valley bottom to higher altitudes. Therefore, we selected lower elevation areas in the valley bottom as the source region for advected water vapor (Zhang et al., 2021).

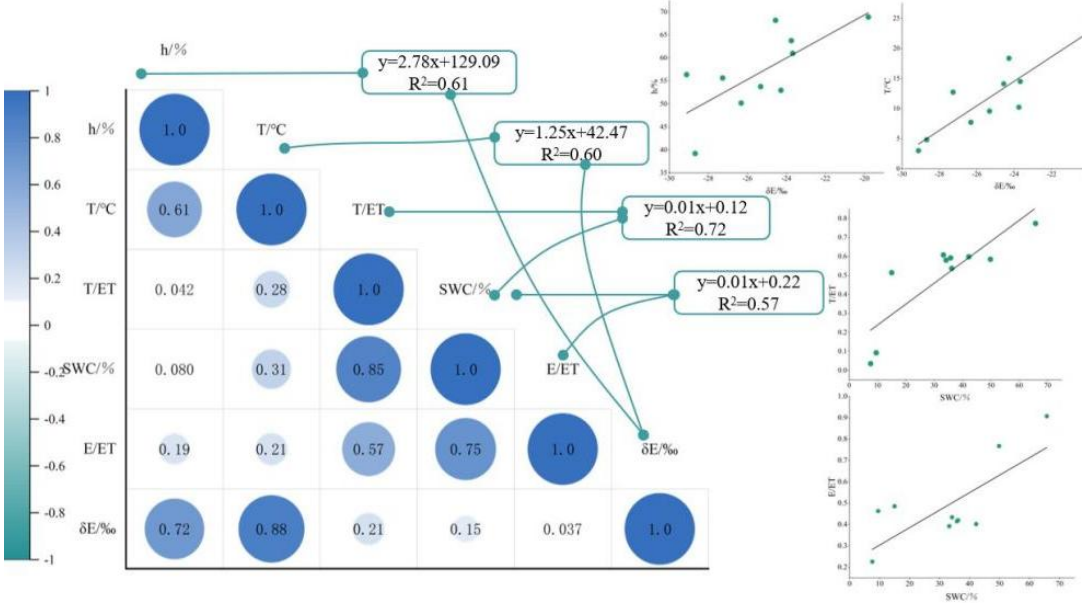

Figure 8:Correlation analysis of factors affecting uncertainty in impact assessment.

6 Conclusions

This study leverages isotopic data from field observations (2018-2022) and model simulations to investigate the dynamics of evapotranspiration in the northeastern Tibetan Plateau, aiming to elucidate its relationship with local water cycling and hydrological impacts. The findings reveal that evaporation and transpiration rates peak during July and August, indicating that transpiration from Picea crassifolia plays a more dominant role than soil evaporation in these periods. Quantitative analysis of plant transpiration and soil evaporation contributions to total evapotranspiration yielded an average T/ET ratio of 0.57 over the study period, reaching a maximum of 0.77 in July. Consequently, it is evident that transpiration by forest trees is the primary component of evapotranspiration within the Picea crassifolia ecosystem. Further examination of the hydrological effects associated with Picea crassifolia evapotranspiration demonstrates that monthly evapotranspiration

https://doi.org/10.5194/egusphere-2024-2246
Preprint. Discussion started: 19 August 2024

volumes are at least threefold higher than precipitation, significantly limiting the potential for surface runoff formation in this region. Comparative analysis of atmospheric water vapor contributions from precipitation across spring, summer, and autumn reveals that the June to August period marks the peak transpiration season for Picea crassifolia, contributing up to 25% of total atmospheric water vapor, whereas surface evaporation accounts for only 18%. Within the 2543 to 3448m elevation range,the average value of *f*re is 28%, it is indicated that the water vapor cycle generated by vegetation evapotranspiration has increased the total precipitation in high-altitude mountain areas. In light of global warming, drought, water scarcity, and climate changes driven by relative humidity alterations have significantly impacted the ecological communities, ecosystem functions, services, and land-climate interactions of Picea crassifolia. It is imperative to recognize the critical role of evapotranspiration in depleting rainfall within this forest belt, underscoring its significance for local water resource management and ecological conservation.

Data availability

The data that support the findings of this study are available on request from the corresponding author, stable isotope data are not publicly available due to privacy or ethical restrictions. Potential evapotranspiration and surface evapotranspiration data are available from the National Tibetan Plateau Scientific Data Centre(TPDC).

Author contribution

Yinying Jiao and Guofeng Zhu conceived the idea of the study; Gaojia Meng, Siyu Lu analyzed the data; Dongdong Qiu, Qinqin Wang, Rui Li, Longhu Chen participated in the drawing; Yinying Jiao wrote the paper; Wentong Li checked the format. All authors discussed the results and revised the manuscript.

Competing interests

The authors declare that they have no conflict of interest.

Acknowledgements

This research was financially supported by the National Natural Science Foundation of China (42371040, 41971036), the Key Natural Science Foundation of Gansu Province (23JRRA698), the Key Research and Development Program of Gansu Province (22YF7NA122), the Cultivation Program of Major key projects of Northwest Normal University (NWNU-LKZD-202302), the Oasis Scientific Research achievements Breakthrough Action Plan Project of Northwest Normal University (NWNU-LZKX-202303).

https://doi.org/10.5194/egusphere-2024-2246
Preprint. Discussion started: 19 August 2024

References

Aron, P. G., Poulsen, C. J., Fiorella, R. P., Matheny, A. M., and Veverica, T. J.: An isotopic approach to partition evapotranspiration in a mixed deciduous forest, 13, https://doi.org/10.1002/eco.2229, 2020.

Ault, T. R.: On the essentials of drought in a changing climate, 368, 256–260, https://doi.org/10.1126/science.aaz5492, 2020.

Brubaker, K. L., Entekhabi, D., and Eagleson, P. S.: Estimation of Continental Precipitation Recycling, 6, 1077–1089, 1993.

Ding, Y. and Peng, S.: Spatiotemporal Trends and Attribution of Drought across China from 1901–2100, 12, 477, https://doi.org/10.3390/su12020477, 2020.

Ding, Y. and Peng, S.: Spatiotemporal change and attribution of potential evapotranspiration over China from 1901 to 2100, 145, 79–94, https://doi.org/10.1007/s00704-021-03625-w, 2021.

Eisenhauer, N. and Weigelt, A.: Ecosystem effects of environmental extremes, 374, 1442–1443, https://doi.org/10.1126/science.abn1406, 2021.

Gibson, J. J. and Reid, R.: Stable isotope fingerprint of open-water evaporation losses and effective drainage area fluctuations in a subarctic shield watershed, 381, 142–150, https://doi.org/10.1016/j.jhydrol.2009.11.036, 2010.

Gibson, J. J. and Reid, R.: Water balance along a chain of tundra lakes: A 20-year isotopic perspective, 519, 2148–2164, https://doi.org/10.1016/j.jhydrol.2014.10.011, 2014.

Good, S. P., Soderberg, K., Wang, L., and Caylor, K. K.: Uncertainties in the assessment of the isotopic composition of surface fluxes: A direct comparison of techniques using laser-based water vapor isotope analyzers, 117, https://doi.org/10.1029/2011jd017168, 2012.

Han, J., Tian, L., Cai, Z., Ren, W., Liu, W., Li, J., and Tai, J.: Season-specific evapotranspiration partitioning using dual water isotopes in a Pinus yunnanensis ecosystem, southwest China, 608, 127672, https://doi.org/10.1016/j.jhydrol.2022.127672, 2022.

Hao, L., Sun, G., Huang, X., Tang, R., Jin, K., Lai, Y., Chen, D., Zhang, Y., Zhou, D., Yang, Z.-L., Wang, L., Dong, G., and Li, W.: Urbanization alters atmospheric dryness through land evapotranspiration, 6, https://doi.org/10.1038/s41612-023-00479-z, 2023.

Hernández-Pérez, E., Levresse, G., Carrera-Hernández, J., and García-Martínez, R.: Short term evaporation estimation in a natural semiarid environment: New perspective of the Craig – Gordon isotopic model, 587, 124926, https://doi.org/10.1016/j.jhydrol.2020.124926, 2020.

Horita, J. and Wesolowski, D. J.: Liquid-vapor fractionation of oxygen and hydrogen isotopes of water from the freezing to the critical temperature, 58, 3425–3437, https://doi.org/10.1016/0016-7037(94)90096-5, 1994.

Jasechko, S., Sharp, Z. D., Gibson, J. J., Birks, S. J., Yi, Y., and Fawcett, P. J.: Terrestrial water fluxes dominated by transpiration, 496, 347–350, https://doi.org/10.1038/nature11983, 2013.

Kale Celik, S., Madenoglu, S., and Turker, U.: Partitioning evapotranspiration of winter wheat based on oxygen isotope approach under different irrigation regimes, 71, 882–896, https://doi.org/10.1002/ird.2701, 2022.

https://doi.org/10.5194/egusphere-2024-2246
Preprint. Discussion started: 19 August 2024

Keeling, C. D.: The concentration and isotopic abundances of atmospheric carbon dioxide in rural areas, 13, 322–334, https://doi.org/10.1016/0016-7037(58)90033-4, 1958.

Kong, Y., Pang, Z., and Froehlich, K.: Quantifying recycled moisture fraction in precipitation of an arid region using deuterium excess, 65, 19251, https://doi.org/10.3402/tellusb.v65i0.19251, 2013.

Kool, D., Agam, N., Lazarovitch, N., Heitman, J. L., Sauer, T. J., and Ben-Gal, A.: A review of approaches for evapotranspiration partitioning, 184, 56–70, https://doi.org/10.1016/j.agrformet.2013.09.003, 2014.

Li, Z., Ciais, P., Wright, J. S., Wang, Y., Liu, S., Wang, J., Li, L. Z. X., Lu, H., Huang, X., Zhu, L., Goll, D. S., and Li, W.: Increased precipitation over land due to climate feedback of large-scale bioenergy cultivation, 14, https://doi.org/10.1038/s41467-023-39803-9, 2023.

Liu, Y., Kumar, M., Katul, G. G., Feng, X., and Konings, A. G.: Plant hydraulics accentuates the effect of atmospheric moisture stress on transpiration, 10, 691–695, https://doi.org/10.1038/s41558-020-0781-5, 2020.

Liu, Y., Lian, J., Luo, Z., and Chen, H.: Spatiotemporal variations in evapotranspiration and transpiration fraction following changes in climate and vegetation in a karst basin of southwest China, 612, 128216, https://doi.org/10.1016/j.jhydrol.2022.128216, 2022.

Liu, Y., Zhuang, Q., Miralles, D., Pan, Z., Kicklighter, D., Zhu, Q., He, Y., Chen, J., Tchebakova, N., Sirin, A., Niyogi, D., and Melillo, J.: Evapotranspiration in Northern Eurasia: Impact of forcing uncertainties on terrestrial ecosystem model estimates, 120, 2647–2660, https://doi.org/10.1002/2014jd022531, 2015.

Maxwell, R. M. and Condon, L. E.: Connections between groundwater flow and transpiration partitioning, 353, 377–380, https://doi.org/10.1126/science.aaf7891, 2016.

Mehmood, S., Ashfaq, M., Kapnick, S., Gosh, S., Abid, M. A., Kucharski, F., Batibeniz, F., Saha, A., Evans, K., and Hsu, H.-H.: Dominant controls of cold-season precipitation variability over the high mountains of Asia, 5, https://doi.org/10.1038/s41612-022-00282-2, 2022.

Peng, S., Ding, Y., Liu, W., and Li, Z.: 1 km monthly temperature and precipitation dataset for China from 1901 to 2017, 11, 1931–1946, https://doi.org/10.5194/essd-11-1931-2019, 2019.

Peng, S., Ding, Y., Wen, Z., Chen, Y., Cao, Y., and Ren, J.: Spatiotemporal change and trend analysis of potential evapotranspiration over the Loess Plateau of China during 2011–2100, 233, 183–194, https://doi.org/10.1016/j.agrformet.2016.11.129, 2017.

Raz-Yaseef, N., Rotenberg, E., and Yakir, D.: Effects of spatial variations in soil evaporation caused by tree shading on water flux partitioning in a semi-arid pine forest, 150, 454–462, https://doi.org/10.1016/j.agrformet.2010.01.010, 2010.

Rohatyn, S., Yakir, D., Rotenberg, E., and Carmel, Y.: Limited climate change mitigation potential through forestation of the vast dryland regions, 377, 1436–1439, https://doi.org/10.1126/science.abm9684, 2022.

Sang, L., Zhu, G., Xu, Y., Sun, Z., Zhang, Z., and Tong, H.: Effects of Agricultural Large-And Medium-Sized Reservoirs on Hydrologic Processes in the Arid Shiyang River Basin, Northwest China, 59, https://doi.org/10.1029/2022wr033519, 2023.

https://doi.org/10.5194/egusphere-2024-2246
Preprint. Discussion started: 19 August 2024

Skrzypek, G., Mydłowski, A., Dogramaci, S., Hedley, P., Gibson, J. J., and Grierson, P. F.: Estimation of evaporative loss based on the stable isotope composition of water using Hydrocalculator, 523, 781–789, https://doi.org/10.1016/j.jhydrol.2015.02.010, 2015.

Su Tao, Lu Zhen-Yu, Zhou Jie, Hou Wei, Li Yue, and Tu Gang: Spatial distribution and seasonal variation characteristics of global atmospheric moisture recycling, 63, 099201, https://doi.org/10.7498/aps.63.099201, 2014.

Sun, X., Wilcox, B. P., and Zou, C. B.: Evapotranspiration partitioning in dryland ecosystems: A global meta-analysis of in situ studies, 576, 123–136, https://doi.org/10.1016/j.jhydrol.2019.06.022, 2019.

Tague, C. L., Moritz, M., and Hanan, E.: The changing water cycle: The eco-hydrologic impacts of forest density reduction in Mediterranean (seasonally dry) regions, 6, https://doi.org/10.1002/wat2.1350, 2019.

Wang, P., Yamanaka, T., Li, X.-Y., and Wei, Z.: Partitioning evapotranspiration in a temperate grassland ecosystem: Numerical modeling with isotopic tracers, 208, 16–31, https://doi.org/10.1016/j.agrformet.2015.04.006, 2015.

Wang, S., Wang, L., Zhang, M., Shi, Y., Hughes, C. E., Crawford, J., Zhou, J., and Qu, D.: Quantifying moisture recycling of a leeward oasis in arid central Asia using a Bayesian isotopic mixing model, 613, 128459, https://doi.org/10.1016/j.jhydrol.2022.128459, 2022.

Wei, Z., Lee, X., Wen, X., and Xiao, W.: Evapotranspiration partitioning for three agro-ecosystems with contrasting moisture conditions: a comparison of an isotope method and a two-source model calculation, 252, 296–310, https://doi.org/10.1016/j.agrformet.2018.01.019, 2018.

Wyatt, C. J. W., O'Donnell, F. C., and Springer, A. E.: Semi-Arid Aquifer Responses to Forest Restoration Treatments and Climate Change, 53, 207–216, https://doi.org/10.1111/gwat.12184, 2014.

Yao, Y., Liang, S., Li, X., Chen, J., Liu, S., Jia, K., Zhang, X., Xiao, Z., Fisher, J. B., Mu, Q., Pan, M., Liu, M., Cheng, J., Jiang, B., Xie, X., Grünwald, T., Bernhofer, C., and Roupsard, O.: Improving global terrestrial evapotranspiration estimation using support vector machine by integrating three process-based algorithms, 242, 55–74, https://doi.org/10.1016/j.agrformet.2017.04.011, 2017.

Yepez, E. A., Huxman, T. E., Ignace, D. D., English, N. B., Weltzin, J. F., Castellanos, A. E., and Williams, D. G.: Dynamics of transpiration and evaporation following a moisture pulse in semiarid grassland: A chamber-based isotope method for partitioning flux components, 132, 359–376, https://doi.org/10.1016/j.agrformet.2005.09.006, 2005.

Zhang, M. and Wei, X.: Deforestation, forestation, and water supply, 371, 990–991, https://doi.org/10.1126/science.abe7821, 2021.

Zhang, R., Xu, X., Liu, M., Zhang, Y., Xu, C., Yi, R., and Luo, W.: Comparing evapotranspiration characteristics and environmental controls for three agroforestry ecosystems in a subtropical humid karst area, 563, 1042–1050, https://doi.org/10.1016/j.jhydrol.2018.06.051, 2018.

Zhang, Y., Gentine, P., Luo, X., Lian, X., Liu, Y., Zhou, S., Michalak, A. M., Sun, W., Fisher, J. B., Piao, S., and Keenan, T. F.: Increasing sensitivity of dryland vegetation greenness to precipitation due to rising atmospheric CO2, 13, https://doi.org/10.1038/s41467-022-32631-3, 2022.

https://doi.org/10.5194/egusphere-2024-2246
Preprint. Discussion started: 19 August 2024

Zhang, Z., Zhu, G., Pan, H., Sun, Z., Sang, L., and Liu, Y.: Quantifying Recycled Moisture in Precipitation in Qilian Mountains, 13, 12943, https://doi.org/10.3390/su132312943, 2021.

Zhu, G., Guo, H., Qin, D., Pan, H., Zhang, Y., Jia, W., and Ma, X.: Contribution of recycled moisture to precipitation in the monsoon marginal zone: Estimate based on stable isotope data, 569, 423–435, https://doi.org/10.1016/j.jhydrol.2018.12.014, 2019.

Zhu, G., Liu, Y., Shi, P., Jia, W., Zhou, J., Liu, Y., Ma, X., Pan, H., Zhang, Y., Zhang, Z., Sun, Z., Yong, L., and Zhao, K.: Stable water isotope monitoring network of different water bodies in Shiyang River basin, a typical arid river in China, 14, 3773–3789, https://doi.org/10.5194/essd-14-3773-2022, 2022.